JOURNAL OF THERMOPHYSICS AND HEAT TRANSFER
Vol. 23, No. 3, July–September 2009

New Defrosting Method Using Jet Impingement for Precooled Turbojet Engines

Katsuyoshi Fukiba*
Muroran Institute of Technology, Muroran, Hokkaido 050-8585, Japan
Shou Inoue† and Hidetoshi Ohkubo‡
Tamagawa University, Machida, Tokyo 194-8610, Japan
and
Tetsuya Sato§
Waseda University, Shinjyuku-ku, Tokyo 169-8555, Japan

DOI: 10.2514/1.40491

Precooled turbojet engines are effective propulsion systems for hypersonic aircraft. However, a serious problem is that frost forms on the cooling tubes of the precooler, thereby decreasing the engine performance. This paper presents a new method for defrosting the precooler using jet impingement. The validity of the proposed defrosting method was investigated through fundamental experiments. In the experiments, the frost formed on the cooling tubes of the single-row heat exchanger was removed by jet impingement. We used the jet periodically. The jet interval is 10–50 s. In addition, the jet duration is short (about 0.1 s). Therefore, the consumption of the high-pressure air to make the jet flow is small. The coolant temperature and main flow speed influences on the defrosting method effectiveness were assessed. Results show that this defrosting method is effective, especially when the coolant temperature and the main flow speed are low.

Nomenclature

A	=	area of cross section, m^2
c_p	=	specific heat at constant pressure, J/kg/K
m	=	mass flow rate of main air, kg/s
m_j	=	mass flow rate of jet, kg/s
$p_{0\text{in}}$	=	total pressure at the inlet, Pa
$p_{0\text{out}}$	=	total pressure at the outlet, Pa
Q	=	heat transfer rate, W
T_{in}	=	airflow temperature at the inlet, K
T_{out}	=	airflow temperature at the outlet, K
u_∞	=	main airflow speed, m/s
Δc_p	=	pressure loss coefficient
ρ_∞	=	main airflow density, kg/m^3
ϕ	=	ratio of mass flow rate of jet to main air

I. Introduction

PRECOOLED turbojet engines have a heat exchanger (precooler) to cool the breathed air using cryogenic fuel as the coolant. The engines exhibit improved performance by cooling of the air. Precooled turbojet engines are effective as a propulsion system for supersonic or hypersonic aircraft. The Japan Aerospace Exploration Agency (JAXA) has conducted development studies of the engines for a decade [1,2]. Results show that frost formation on the cooling tubes of the precooler is a serious impediment to performance. Figure 1 shows a precooler installed in our ATREX engine, an air breathing engine developed by JAXA [3]. Magnified images of the cooling tubes in the firing test are also presented in Fig. 1b. Immediately after starting the firing test, frost started to build up on the cooling tubes. After 90 s, the flowpath of the precooler was almost closed by frost formation. This frost formation problem must be solved if we want to use precoolers in flight.

Many precedent studies have described frost formation of heat exchangers [4]. Most studies were undertaken by application of air conditioners. Many ideas have also been put forward to address the frost formation problem [5]. However, those ideas fundamentally require increased weight of the system. For example, a defrosting method to melt the frost by heat addition is often used for heat exchangers on the ground. The disadvantage of this method is that we cannot use the heat exchanger during defrosting. We must then install a redundant heat exchanger if we want to cool the air continuously. This greatly increases the weight of the system. A defrosting method using alcohol spray was proposed in previous development studies of precooled turbojet engines. Harada et al. [6], Kimura and Sato [7], and Sato et al. [8] studied the defrosting method and created a method to partially remove the frost. However, this method necessitates installation of an alcohol tank and the spraying devices, which also increases weight. Such a weight increase of the system is fatal to the engine and aircraft.

In this paper, a defrosting method using jet impingement on the cooling tubes is proposed. Figure 2 shows a schematic diagram of a precooled turbojet engine with the installed defrosting devices. The cryogenic fuel passes through the precooler upstream of the compressor and cools the main air. The high-speed air jet is impinged on the cooling tubes of the precooler, thereby removing the frost. Using the high-pressure air downstream of the compressor, we can minimize the weight increase of the engine. This method merely requires pipes, valves, and nozzles to guide the jet.

This paper presents results of our fundamental studies of the jet defrosting method. The effectiveness of the jet defrosting method was investigated using a small, single-row heat exchanger and an air conditioner. First, we used liquid nitrogen as the coolant to make the surface temperature about 80 K. In previous studies, Ohkubo and Tajima studied frost formation on a vertical flat plate whose surface temperatures were 80–270 K [9]. In that study, they classified the surface temperatures into four classes. According to their classification, the surface temperature of 80 K belongs in the fourth

Received 19 August 2008; revision received 25 December 2008; accepted for publication 30 March 2009.

*Assistant Professor, Aerospace Plane Research Center, 27-1 Mizumoto-chou.
†Graduate Student, Department of Mechanical Engineering, 6-1-1 Tamagawa-gakuen, Machida.
‡Professor, Department of Mechanical Engineering, 6-1-1 Tamagawa-gakuen, Machida.
§Professor, Department of Applied Mechanics and Aerospace Engineering, 3-4-1 Ohkubo, Shinjuku-ku. Member AIAA.

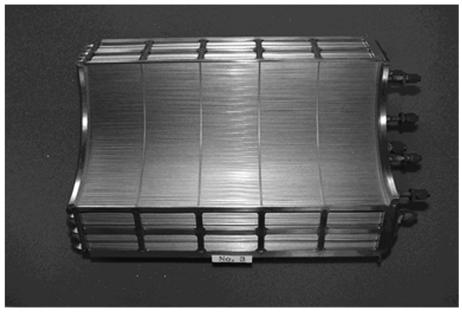

a) Precooler element

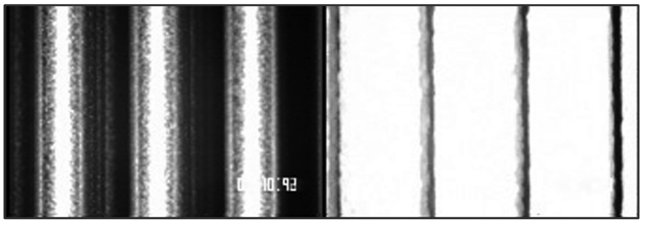

b) Magnified images of the cooling tubes

Fig. 1 Cooling tubes of the precooler before (left) and after (right) the firing test.

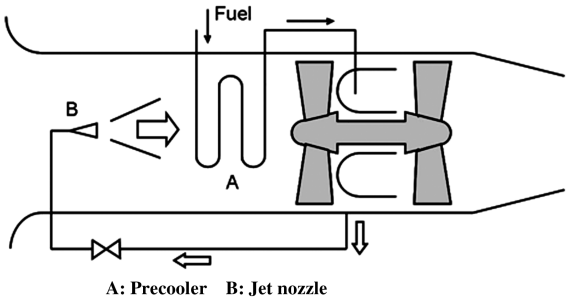

A: Precooler B: Jet nozzle

Fig. 2 Schematic diagram of a precooled turbojet engine with jet defrosting devices.

class, which includes surface temperatures of 80–160 K. The frost forming on the surface of the fourth class shows unique characteristics. For example, the mass flux of the frost is much smaller than that in the other classes. However, data of the frost formation on heat exchangers in this class are not presented well. One of the few reports describing frost in this class was presented by Harada et al. [6,10]. Harada pointed out that the frost in this class is less dense and fragile. This feature seems to provide advantages for jet defrosting. Next, we used hydrofluoroether as the coolant to render the surface temperature as either 220 or 250 K. In this case, the surface temperatures are classified as first and second class. In these classes, the frost is denser than that in the fourth class: the frost in the first and second class is firm. The effect of the surface temperature on the effectiveness of jet defrosting was investigated. Finally, experiments at various airflow speeds were also conducted. Through these tests, the effect of the airflow speed was investigated.

II. Experimental Setup

Figure 3 depicts the experimental apparatus used for this study. The apparatus comprises an air conditioner (A), a duct with a honeycomb section (B), and a test section including the jet supply system and a heat exchanger. Air of constant temperature and humidity is provided by the air conditioner to the test section through the honeycomb section. A hot wire anemometer and thermocouple are placed in the test section inlet. For the anemometer, we used an off-the-shelf model (Model 6531, Kanomax). The response speed is 1.0 s according to its specification. The total uncertainty of the flow speed measurement is ± 0.13 m/s root sum square (RSS) [11]. However, it consists of the bias uncertainty of 0.10 and the precision uncertainty of 0.03. In the case of this study, most results will be shown in a comparative style. In such comparative tests, we can neglect the bias uncertainty.

The duct of the test section is transparent acrylic resin with a 60×60 mm square cross section. The downstream of the heat exchanger has two thermocouples. The distances from the lower wall to the thermocouples are 10 and 50 mm, respectively. The diameters of the thermocouples are 0.25 mm. Two total pressure measurement ports are located at the upstream and downstream of the heat exchanger. These ports are used for measurement of the heat exchanger's pressure loss. The total uncertainty of the pressure difference measurement is ± 0.5 Pa RSS.

The jet supply system comprises a valve, nozzle, gas feed line, and dry gas nitrogen cylinder. The high-pressure nitrogen is provided from the cylinder to the valve. When the valve opens, the jet is ejected from the nozzle. The nitrogen pressure is 0.6 MPa at the valve inlet. Figure 4 shows a cross section of the jet nozzle located in the test section. For the nozzle, we used the 1/4–1/8 inch Swagelok reducing union. The shape of this union resembles that of a converging–diverging nozzle, as depicted in Fig. 4. The nozzle throat diameter is 2.3 mm. This diameter is larger than the equivalent

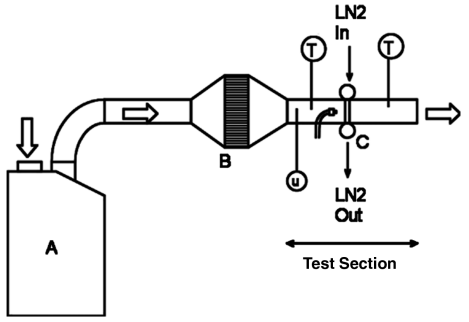

a) Overall setup

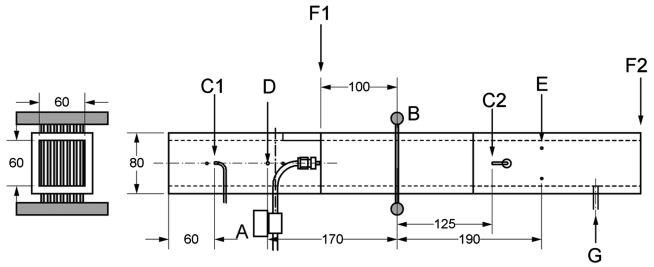

A: nozzle and valve
B: heat exchanger
C1 and C2: pressure measurement port 1 and 2
D: flow speed measurement point
E: thermocouples
F1: nozzle exit and partition
F2: partition
G: purge gas inlet

b) Test section

Fig. 3 Experimental setup.

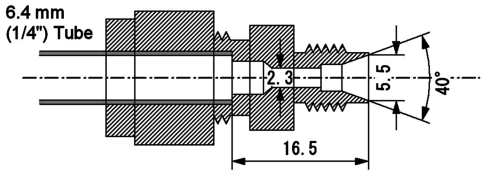

Fig. 4 Cross section of the jet nozzle.

diameter of the electric valve: 1.5 mm. Therefore, the flow chokes at the valve. The nozzle exit is located 100 mm upstream of the heat exchanger. The jet is ejected at the center of the cross section; its direction is parallel to the flowpath. Figure 5a portrays the velocity distribution of the jet measured using a Pitot tube. The Pitot tube was located at 100 mm from the nozzle exit. This measurement was conducted without the duct and heat exchanger. The maximum speed of the jet was 35.8 ± 0.8 m/s.

In this experiment, the minimum jet duration is 0.05 s. It is so short that it might cause a delay because of the valve response. Therefore, we checked the unsteady response of the jet. Figure 5b shows results of the test. In this test of high frequency, a flush mounted pressure transducer was placed at the nozzle exit. The transducer output was recorded at 1000 Hz when the open commands of 0.05, 0.1, and 0.5 s were given. For the pressure transducer, we used XT-140M-100 psi (Kulite Semiconductor Products, Inc.). The resonance frequency of the pressure transducer is 400 kHz. As shown in Fig. 5b, we found that it takes about 0.01 s for the pressure to rise to 90% of the steady condition. It takes 0.1 s for the pressure to reach a steady state. Therefore, for 0.05 s, we use the transient state to eject the jet. The response to close the valve is good. The valve closing duration is within 0.01 s.

Figure 6 shows the heat exchanger we used in this experiment. The heat exchanger consists of manifolds, which are the 5/8 inch tubes, and seven stainless steel cooling tubes, whose diameters and thickness are 4 and 0.5 mm, respectively. The distances between the cooling tubes are 4.6 mm (L2 in Fig. 6); the distance from each tube to the side wall is 2.3 mm (L1 and L8 in Fig. 6).

The test conditions of this study are presented in Table 1. The main flow speed is set to the prescribed value shown in Table 1 before cooling starts in each case. After the test starts, frost starts to build up on the heat exchanger cooling tubes. The frost causes the pressure loss of the heat exchanger. Therefore, the flow speed starts to decrease after the test starts. The highest limit of the flow speed is 3.0 m/s in our test, which is limited by the air conditioner ability. This flow speed may seem to be slow compared with that of the actual engine. However, in the actual engine the flow speed at the precooler is designed to be slow to reduce the pressure loss. For example, the cross section of the precooler installed in the ATREX engine [8] is shown in Fig. 7. In the case of the ATREX engine, the cross-sectional area of the flowpath at the compressor entrance is 0.076 m^2. On the other hand, the cross-sectional area of the flowpath at the precooler entrance is 0.96 m^2. The normal mass flow rate of the ATREX engine is 8.0 kg/s. Therefore, the flow speed at the precooler entrance is 7.1 m/s at ground test condition if the flow is uniform. The flow

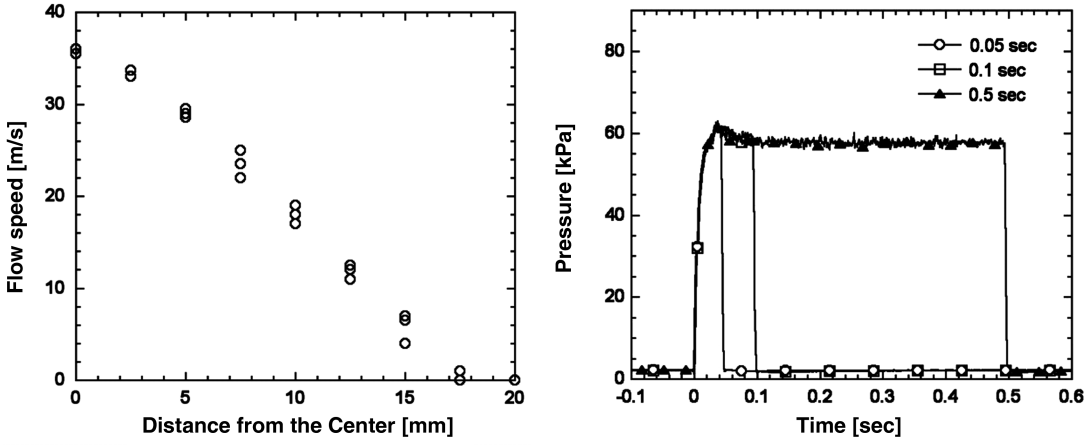

a) Distribution of the flow speed **b) Unsteady behavior of the jet**

Fig. 5 Flow properties of the jet.

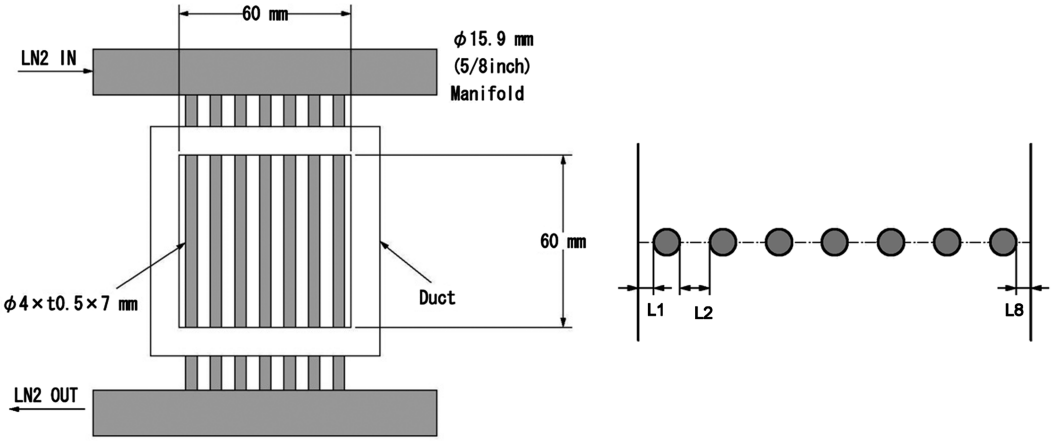

a) Cross section of the heat exchanger **b) Distance between tubes**

Fig. 6 Geometry of the heat exchanger.

Table 1 Experimental conditions

Case	1	2	3	4	5
Coolant temperature, K	83	←	←	220	250
Main flow speed, m/s	1.0	2.0	3.0	1.0	1.0
Flow temperature, K	296.15	←	←	←	←
Flow humidity, %	59	←	←	←	←

speed of this fundamental study is a little bit slower than that of the actual precooler. However, we think the qualitative performance of the defrosting effect can be demonstrated. In the ATREX firing test, the frost formed on the precooler tubes has hardly blown off by the main airflow itself.

Coolant of two kinds was used in this experiment: liquid nitrogen and hydrofluoroether. In Cases 1, 2, and 3, we used liquid nitrogen as the coolant. The liquid nitrogen was provided using the self-pressurized tank. The provided pressure is about 0.15 MPa. The boiling point of the liquid nitrogen increases concomitantly with the tank pressure. The inlet and outlet temperatures of the liquid nitrogen measured using thermocouples were 83 K. No temperature difference was observed between the inlet and outlet. The cooling tube thickness was 0.5 mm. The temperature increase from the coolant to the outside surface was estimated as 0.5 K according to the theory of heat conduction. Therefore, the surface temperature of the cooling tubes was estimated as 83.5 ± 1 K. In Cases 4 and 5, we used hydrofluoroether (Novec 7200; 3M, Inc.) as the coolant. The schematic diagram of the coolant circulation system is portrayed in Fig. 8. The coolant is circulated with the magnet pump. The heat exchanger inserted in the line (A in Fig. 8) cools the coolant to the prescribed temperature. The heat exchanger exchanges the heat between the coolant and liquid nitrogen. The lower limit of the coolant temperature produced by this system is about 200 K.

The test procedure is the following:

1) Partition plates, which separate the area around the heat exchanger, are inserted upstream and downstream of the heat exchanger.

2) Dry nitrogen gas is injected in the area separated by the plates.

3) Cooling is started by providing coolant to the heat exchanger.

4) In 5 min, the coolant temperature of the cooling tubes becomes steady.

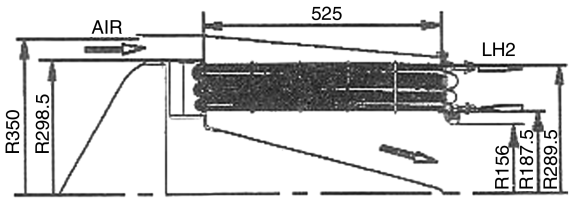

Fig. 7 Cross section of the precooler installed the ATREX engine.

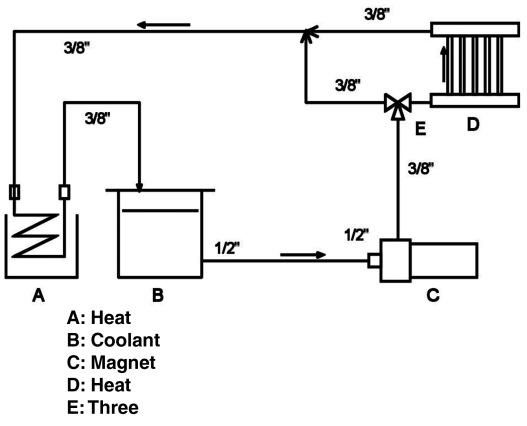

Fig. 8 Coolant circulation system.

5) Injection of nitrogen gas is stopped. We remove the partition plates. Then the test starts.

Finally, for this experiment, all parameters (pressure, temperature, and flow speed) were changed from analog data to digital data and recorded at 5 Hz.

III. Results

A. Without Jet, Coolant Temperature of 83 K

The features of heat transfer without jet defrosting are presented next. Figure 9 shows cooling tubes of the heat exchanger at the start, and at 50 s and 250 s after the test started. Immediately after the test started, frost formation on the cooling tubes was observed. The frost grew with time and eventually closed the heat exchanger flowpath. Figure 10 shows variations of the airflow speed u_∞ and the air temperature downstream of the heat exchanger T_{out}. In this figure, three results recorded under the same condition are shown to evaluate the reproducibility of the measurements. Immediately after the test started, the flow speed measured using the anemometer also started to decrease because of the increase in the pressure loss attributable to the frost formation. The flow speed continues to decrease with time; eventually, it becomes zero at about 250 s. Furthermore, T_{out} increases from the test start to 20 s. However, it changes its gradient and starts to decrease after 20 s. This is true because, initially, the decrease in the heat transfer rate attributable to the heat resistance of the frost increases T_{out}. Then the flow speed decreases gradually, which reflects the decrease in the mass flow rate of the air. As a result, T_{out} starts to decrease after 20 s although the heat transfer rate decreases. Regarding reproducibility, for 0–150 s the three data cluster well. The three u_∞ cluster within 0.1 m/s, and the three T_{out} within 1.0 K. After 150 s, the disturbance of u_∞ and T_{out} becomes large. During this period, some inconsistency is apparent locally because the flow becomes easy to disturb as a result of the flow speed decrease.

The heat transfer rate Q is calculated as follows.

$$Q = \rho_\infty u_\infty A c_p (T_{\text{in}} - T_{\text{out}}) \tag{1}$$

It seemed that T_{out} might vary widely from point to point in a cross section. For that reason, a primary test was conducted using the

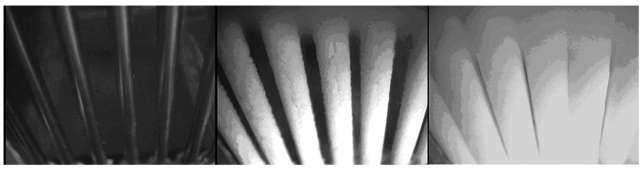

Fig. 9 Cooling tubes at the test start, 50, and 250 s after the test start.

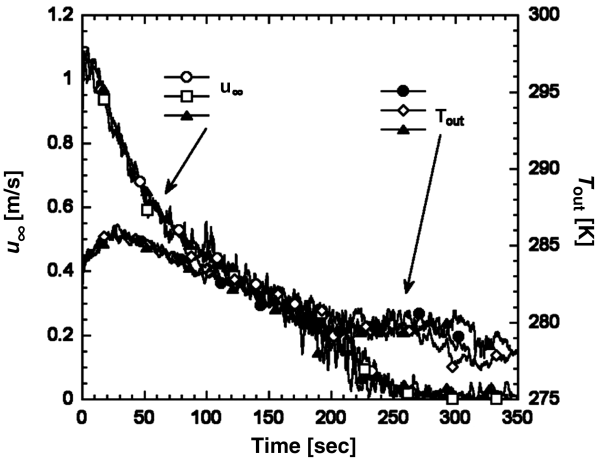

Fig. 10 Variation of the flow speed and the air temperature downstream of the heat exchanger.

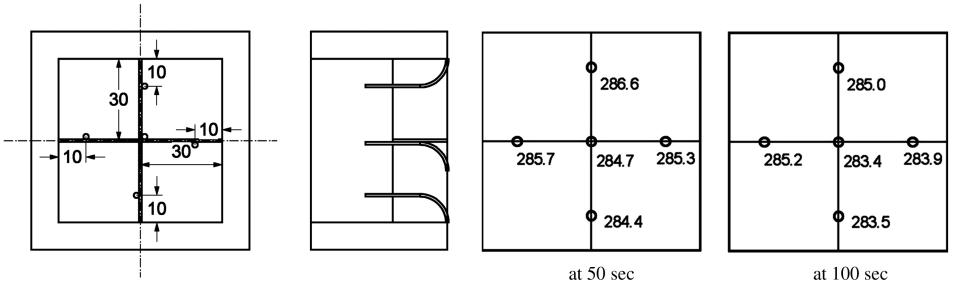

a) Thermocouple rack **b) Air temperature distribution**

Fig. 11 Air temperature distribution downstream of the heat exchanger.

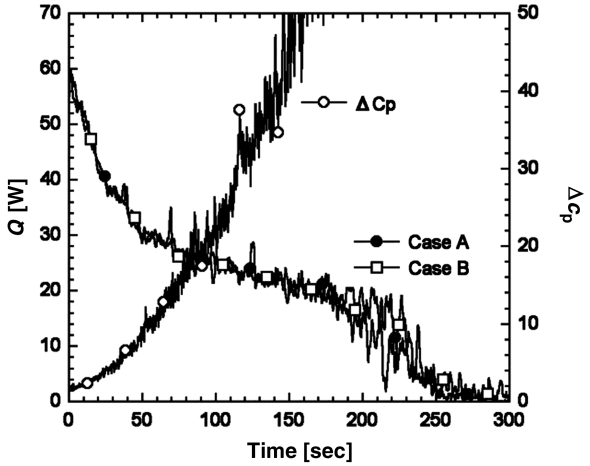

Fig. 12 Variation of the heat transfer rate and the pressure loss coefficient.

thermocouple rake presented in Fig. 11. This thermocouple rake has five thermocouples and can therefore measure the temperature distribution in the cross section. Results show that the variation between points in the cross section is negligible, aside from the variation between upper and lower points. Figure 12 shows two lines of Q, which are Case A and Case B. Case A was obtained using the average T_{out} measured using two thermocouples, which are at 10 mm and 50 mm from the lower wall. Case B was obtained using the average T_{out} measured using the thermocouple rake with its five thermocouples. The two Q values are consistent until about 200 s, where the flow speed slows. Considering these results, we used two thermocouples for the experiment described below.

The following equation was used to calculate the pressure loss coefficient Δc_p:

$$\Delta c_p = \frac{(p_{0\text{in}} - p_{0\text{out}})}{1/2\rho_\infty u_\infty^2} \tag{2}$$

In Fig. 12, the pressure loss coefficient increases monotonously with time. This increase is because of the frost formation.

B. With Jet, Coolant Temperature of 83 K

Figure 13 portrays the cooling tubes of the heat exchanger before and after jet impingement. In this case, the jet was ejected after 50 s from the test start; the jet duration is 0.1 s. Scattering of the frost by jet impingement was observed. After the jet impingement, the distance between tubes became as wide as that of the test start, as presented in Fig. 9. As the right picture of Fig. 13 shows, not all frost was removed. A thin frost layer remained on the tubes. However, the remaining frost is sufficiently thin that the heat transfer rate and the pressure loss coefficient recovered remarkably. Figure 14 depicts the variation of the heat transfer rate with jet defrosting. The heat transfer rate without jet defrosting is also presented in Fig. 14. The jet impingement removes the frost; the flow speed recovers. Simultaneously, the airflow temperature downstream of the heat exchanger decreases. Consequently, the heat exchange rate improves. Figure 15 shows variation of the pressure loss coefficient. The pressure loss coefficient also recovers rapidly by the jet impingement every 50 s, demonstrating that the defrosting method using the jet impingement is valid in this condition.

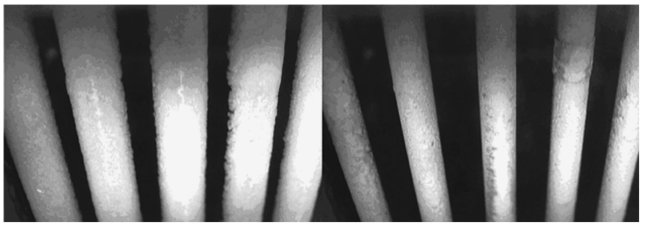

Fig. 13 Cooling tubes before and after the jet impingement.

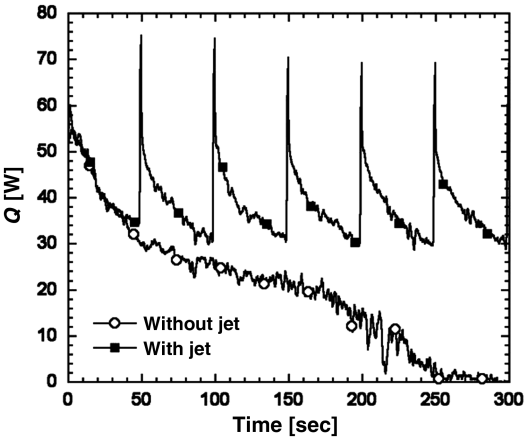

Fig. 14 Variation of the heat transfer rate with jet defrosting.

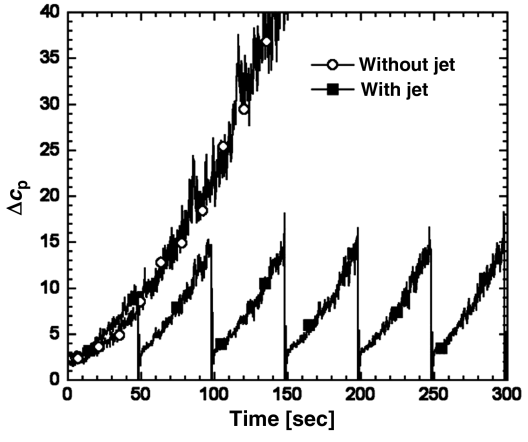

Fig. 15 Variation of the pressure loss coefficient with jet defrosting.

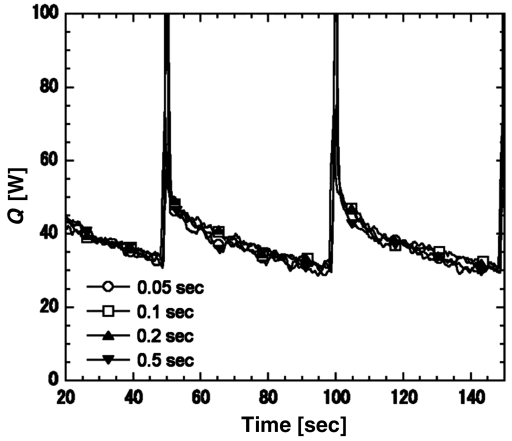

Fig. 16 Effect of the jet duration on the heat transfer rate.

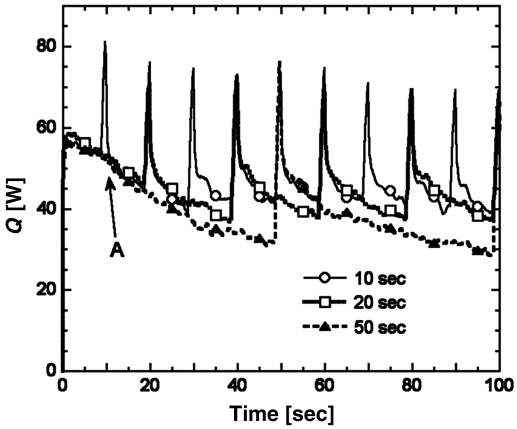

Fig. 17 Effect of the jet interval on the heat transfer rate.

Figure 16 portrays the effect of the jet duration on the heat transfer rate. The jet duration should be as short as possible to reduce the consumption of the high-pressure air. In Fig. 16, the heat transfer rate of 0.5, 0.2, 0.1 and 0.05 s in the jet duration are presented for comparison. These jets were ejected at 50 s and 100 s from the test start. When the jet duration is long, the heat transfer rate immediately after the jet ejection becomes greater than that at the test start (about 60 W) because the air is drawn by the jet and the flow speed increases temporarily. This heat transfer rate increase does not continue for a long time. After a few seconds, it reverts to the same value as that of shorter duration. Consequently, the temporary heat transfer rate increase only slightly affects the total heat transfer rate. Table 2 shows the time averaged heat transfer rate from 0 s to 299 s. The precision uncertainty by three test results of the same condition (the duration is 0.1 s) is 0.7 W. Considering this uncertainty, we found that the jet duration does not affect the average heat transfer rate greatly.

Figure 17 shows the effect of the jet interval on the heat transfer rate. In this figure, the heat transfer rates at 10, 20, and 50 s jet intervals are presented. The jet duration of each ejection is 0.1 s. The average heat transfer becomes larger for shorter intervals. Table 3 shows the time average heat transfer rates from 0–299 s, at 10, 20, and 50 s jet intervals. The time average heat transfer rate at the 10 s interval increases 20% over that at the 50 s interval. However, it is noteworthy here that, in Fig. 17, the heat transfer rate immediately after the first jet defrosting at the 10 s interval is the same as those at 20 and 50 s intervals (point A in Fig. 17). This fact means that this jet defrosting method is not valid until some amount of frost accumulates on the tubes. Therefore, there is a limit to improvement of the heat transfer rate by reducing the interval. In addition, if the jet interval is shortened, we need a larger amount of gas for the jet. The use of high-pressure air downstream of the compressor in gas turbine engines would causes a decrease in the engine performance. Some trade-off pertains when we use jet defrosting in the engine.

Herein, we estimate the air mass flow rate ratio of the jet for defrosting to the main airflow. The mass flow rate of the jet for defrosting m_j is 2.50 g/s if the flow is choked at the electric valve, where the flowpath is the narrowest. On the other hand, the mass flow rate of the main airflow m_∞ is 4.34 g/s when the flow speed is 1.0 m/s. However, the jet is ejected at the intervals of 10 s in the most frequent case and the duration is only 0.1 s. The ratio of the jet to the main airflow in this case is the following:

$$\phi = \frac{\dot{m}_j}{\dot{m}} \times \frac{0.1}{10} = 0.58\% \tag{3}$$

Figure 18 shows the heat transfer rate at which the high-pressure source of the jet is changed from the dry nitrogen cylinder to the humid air, which is made using an off-the-shelf compressor without a dryer. The jet intervals and duration are 50 and 0.1 s, respectively. The room temperature and humidity were 19.6 °C and 41%, respectively, when we conducted the test. The defrosting method proposed in this study is not attributed to the sublimation of the frost, as in the previous study by Inaba et al. [12], but rather the impact power of the jet impingement. Therefore, the effectiveness of this defrosting method is unaffected by the variation of the humidity of the jet air, as presented in Fig. 18. For that reason, this method is effective even if we use humid high-pressure air downstream of the gas turbine compressor for the jet.

C. Effect of the Main Airflow Speed

The effect of the main airflow speed on jet defrosting is investigated next. Figure 19 shows the variation of the flow speed at initial flow speeds of 1.0, 2.0, and 3.0 m/s (Cases 1, 2, and 3 in Table 1), without jet defrosting. The vertical axis is non-dimensionalized by the initial flow speed. About 250 s are necessary for the frost to close the flowpath when the initial flow speed is 1.0 m/s. On the other hand, when the initial flow speed is 2.0 m/s, it takes about 500 s for the flow speed to become 0 m/s. Moreover, when the initial flow speed is 3.0 m/s, the flow speed does not become 0 m/s in the test duration of 500 s. According to these results, we found that the frost growth speed decreases when the flow speed increases under the conditions of this study. Generally, the mass flux of the frost increases concomitantly with the flow speed. This trend is opposite to the trend of the frost growth found in this study. This result means the frost characteristics change with the variation of the flow speed. In this study, the frost becomes denser at higher flow speeds. Consequently, it decreases the growth speed at higher flow speeds.

Figure 20 depicts the variation of the heat transfer rate at the flow speed of 3.0 m/s with and without jet defrosting (Case 3 in Table 1). The difference between the heat transfer rates with and without the jet defrosting is smaller than that at the flow speed of 1.0 m/s, which is mainly because the heat transfer rate without jet defrosting is not so

Table 2 Effect of the jet duration on the average heat transfer rate

Jet duration, s	Average heat transfer rate, W
0.5	39.1
0.2	39.8
0.1	37.9
0.05	38.2

Table 3 Effect of the jet intervals on the average heat transfer rate

Jet intervals, s	Average heat transfer rate, W
10	45.2
20	42.6
30	37.9

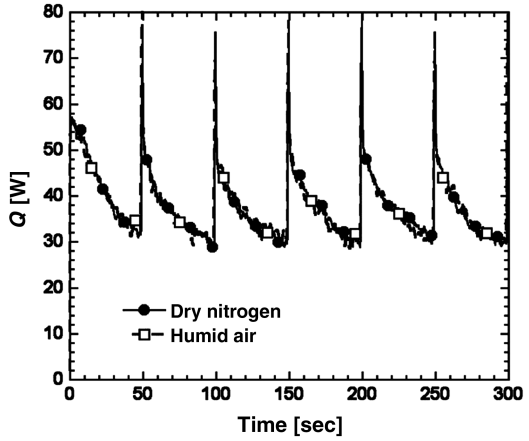

Fig. 18 Effect of the jet humidity.

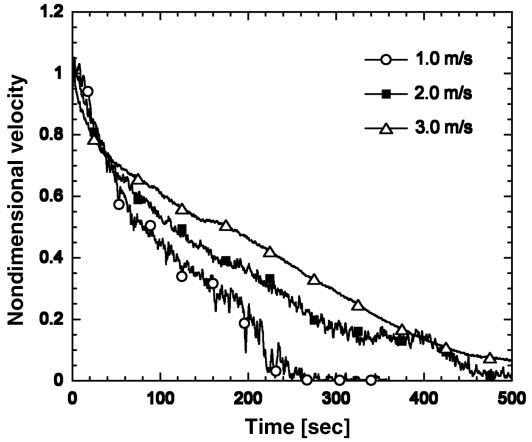

Fig. 19 Nondimensional flow speed at the initial flow speed of 1.0–3.0 m/s.

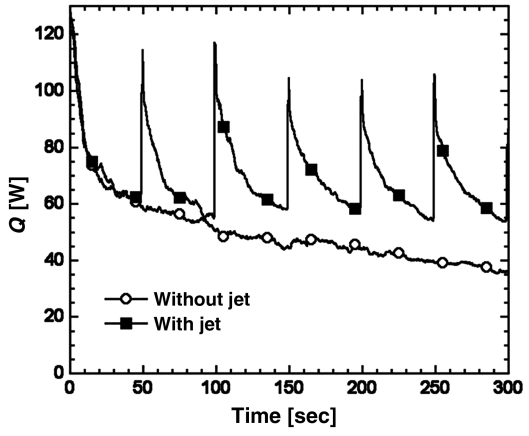

Fig. 20 Variation of the heat transfer rate with jet defrosting. The main airflow speed is 3.0 m/s.

small as that at 1.0 m/s. Figure 21 shows the variation of the pressure loss coefficient Δc_p with and without the jet defrosting. This figure shows that jet defrosting becomes less effective by continued periodic jet ejection. In Fig. 21, Δc_p immediately before the first jet ejection (49 s) is about six. On the other hand, Δc_p immediately before the last jet ejection (299 s) is about 12. This increase in Δc_p results from the accumulation of frost that is not removed in spite of the jet impingement. Figure 22 depicts the heat exchanger immediately after the first jet impingement (50 s) and the sixth jet

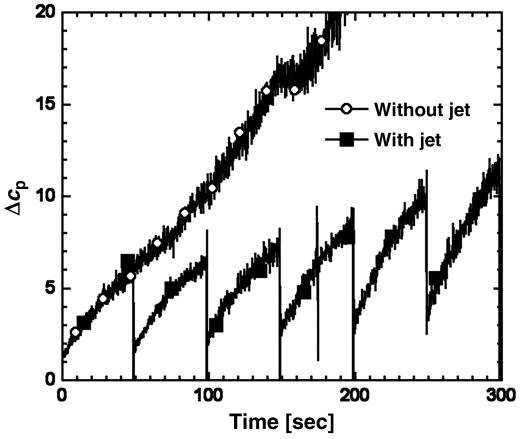

Fig. 21 Pressure loss coefficient with and without jet defrosting. The main airflow speed is 3.0 m/s.

impingement (300 s). Immediately after the first jet impingement, the frost is removed. However, the frost is not cleared off immediately after the sixth jet impingement. Frost remains on the cooling tubes, especially around the corner of the cross section. This phenomenon is not apparent in the experiment at the flow speed of 1.0 m/s. The reason seems to be that the adhesive force of the frost to the cooling tubes increases at the higher flow speed.

The decreased effectiveness of the jet defrosting can be compensated by increasing the jet strength. Figure 23 shows the pressure loss coefficient at the main airflow speed of 3.0 m/s when we change the electric valve of 1.5 mm in the equivalent diameter to that of 3.0 mm. Figure 24 shows the flow speed distribution of the jet with the new electric valve. The jet flow speed was measured 100 mm downstream from the nozzle exit, where the heat exchanger exists. The flow speed is 62.1 ± 0.7 m/s at the center of the cross section. Figure 23 portrays improvement in the pressure loss coefficient using

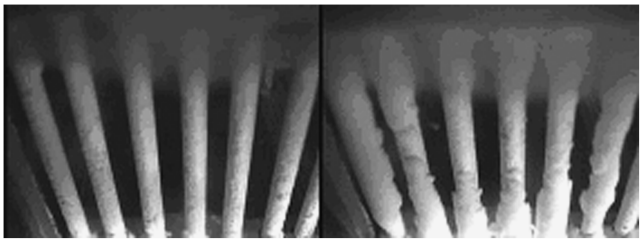

Fig. 22 Pictures of the heat exchanger immediately after the first jet impingement (50 s, left) and the sixth jet impingement (300 s, right).

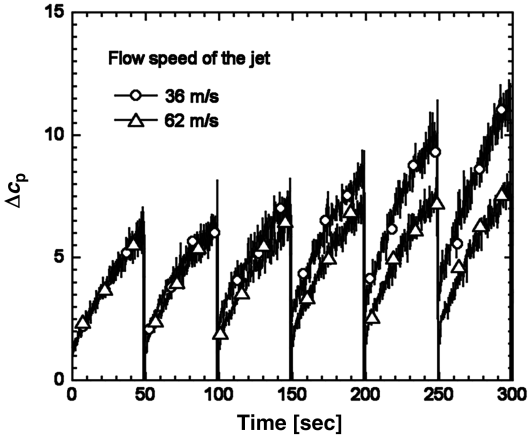

Fig. 23 Effect of the flow speed of the jet on the recovery of the pressure loss coefficient.

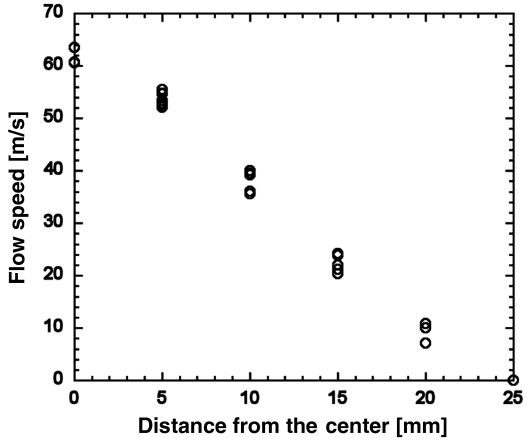

Fig. 24 Flow speed distribution of the strong jet with a large electric valve.

the strong jet. Results show that the defrosting method we proposed is effective under this condition.

D. Effect of Coolant Temperature Variation

This subsection presents investigation of the effect of the variation in coolant temperature. The coolant is changed from liquid nitrogen to the hydrofluoroether to produce coolant temperatures of 220 and 250 K. The coolant circulation system used in the experiment of this subsection is portrayed in Fig. 8. It is noteworthy here that, in this subsection, we do not use the heat transfer rate to evaluate the defrosting method because of the uncertainty of that measurement. When the coolant temperature becomes high, the main air temperature downstream of the heat exchanger also becomes high, causing a small temperature difference between upstream and downstream flows of the heat exchanger. For example, the temperature difference is about 2 K at the coolant temperature of 250 K when the test is started. This engenders an increase in the uncertainty of the heat transfer rate. Therefore, in this subsection, we use the flow speed and the pressure loss coefficient to evaluate the defrosting method.

First, the coolant temperature control accuracy is evaluated. The coolant temperature is controlled by varying the amount of the liquid nitrogen in the coolant and liquid nitrogen heat exchanger (A in Fig. 8). This arrangement of liquid nitrogen is conducted manually. Therefore, some error exists. Figure 25 presents typical results of coolant temperature measurements measured before and after the heat exchanger. In this figure, the objective temperatures are 250 and 220 K. For 250 K as the objective temperature, the maximum temperature is 251 K; the minimum temperature is 248 K throughout the 400 s test. The time average temperatures throughout the test are 249.1 K before the heat exchanger and 250.2 K after the heat exchanger. The precision indexes are 0.6 K and 0.5 K, respectively. The temperature difference between the inlet and outlet is about 1 K. On the other hand, for 220 K, the maximum temperature is 222 K and the minimum temperature is 217 K. The time average temperatures are 218.8 K before the heat exchanger and 221.2 K after the heat exchanger. The precision indexes are 0.8 K and 0.7 K, respectively. The temperature difference between the inlet and outlet is greater than that of 250 K by about 2–3 K.

Figure 26 shows the flow speed profiles without jet defrosting when the coolant temperatures are 83, 220, and 250 K (Cases 1, 4, and 5 presented in Table 1). The initial flow speed is 1.0 m/s in each case. For 83 K, the flow speed decreases rapidly; it becomes 0 m/s in about 250 s. On the other hand, at the coolant temperature of 220 K, the flow speed decrease is slower than that of 83 K. For 250 K, the flow speed decrease is much slower: it decreases to 0.65 m/s in 400 s.

Figure 27 portrays the effect of the coolant temperature on the pressure loss coefficient Δc_p. Results show that the pressure loss increases most rapidly at lower coolant temperature. This results from the difference in the frost growth speed. According to the results of the pressure loss measurement and observation, the frost growth is fastest at the coolant temperature of 83 K and slowest at 250 K. However, results of previous studies show that the mass flux of water vapor becomes lower concomitantly with the surface temperature [9,10]. Apparently, the frost on the lower temperature tubes is less dense.

Figure 28 displays profiles of the flow speed with and without jet defrosting at the coolant temperature of 220 K. In this case, frost scattering by the jet impingement was observed, but the amount of

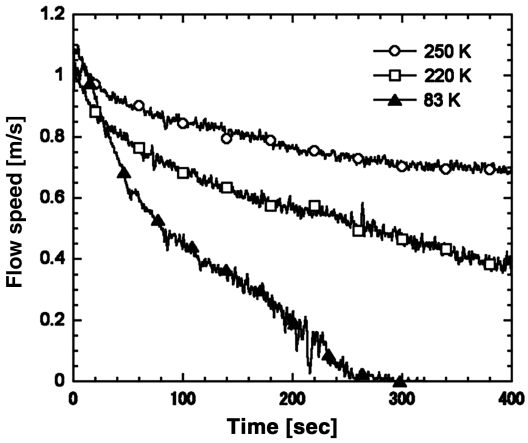

Fig. 26 Effect of the coolant temperature on the flow speed variation.

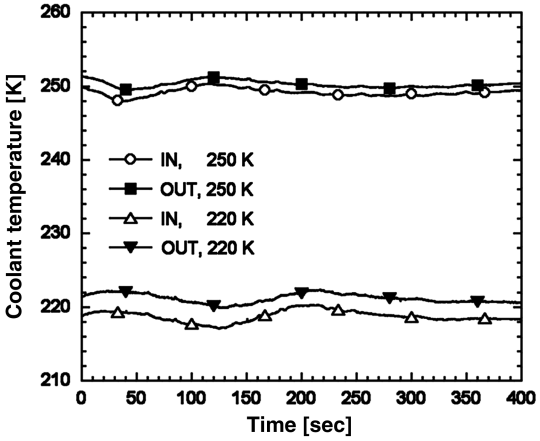

Fig. 25 Coolant temperature measured before and after the heat exchanger.

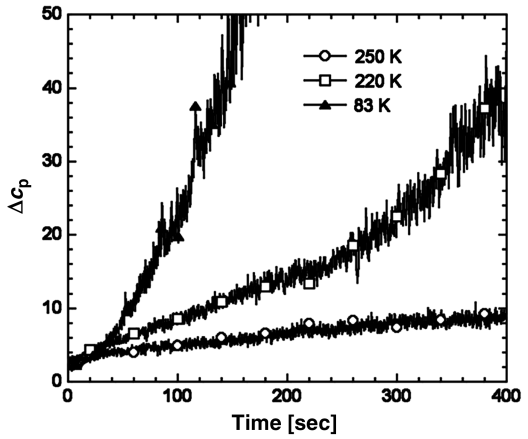

Fig. 27 Effect of the coolant temperature on the pressure loss coefficient.

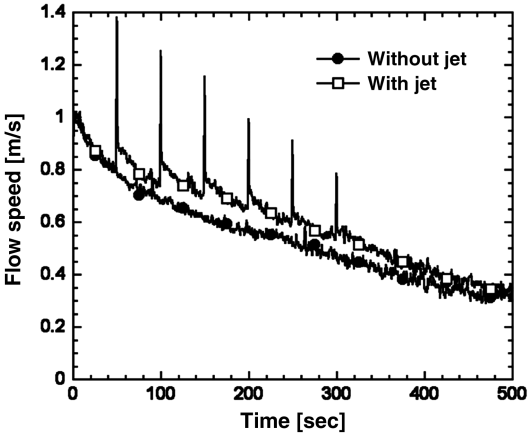

Fig. 28 Main airflow speed profiles with and without jet defrosting at the coolant temperature of 220 K.

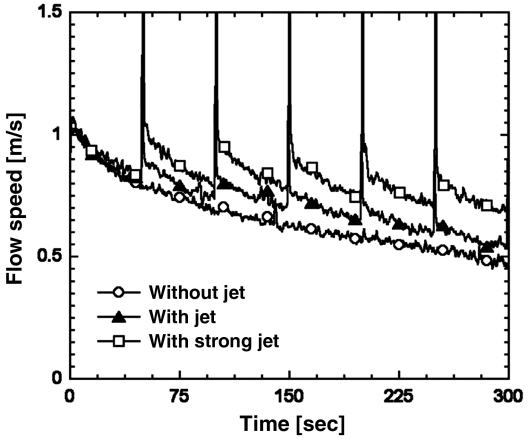

Fig. 31 Main airflow speed profiles with defrosting by the strong jet at the coolant temperature of 220 K.

the scattered frost was small. We also observed that much frost remains on the cooling tubes in spite of the jet impingement. This results in the slight recovery of the flow speed in Fig. 28. Figure 29 presents Δc_p with and without the jet defrosting. We can see slight improvement in Δc_p, but the recovery is less than that at the coolant temperature of 83 K (Fig. 15).

Figure 30 shows the flow speed and Δc_p profiles at the coolant temperature of 250 K. In this case, no difference is observed between these two flow speeds and Δc_p profiles. These results demonstrate that the jet defrosting method is not valid in this condition.

From Figs. 28–30, the following tendency is apparent: when the coolant temperature increases, the jet defrosting method becomes less effective for frost removal. This tendency probably results from the difference of the frost firmness. The frost surface temperature can become greater than the melting point through accumulation of the frost when the coolant temperature is high. In this case, liquid water collects on the frost surface: this water densifies and hardens the frost.

Figure 31 shows flow speed profiles obtained when we use a strong jet. The jet comprises the same devices as those described above (Fig. 24). The coolant temperature and the initial flow speed are 220 K and 1.0 m/s, respectively, in Fig. 31. Use of the strong jet improves the flow speed recovery. This fact demonstrates the possibility of improving the jet defrosting method by changing the jet properties. However, for the 250 K coolant temperature, the main airflow speed and pressure loss coefficient were not recovered even when using the strong jet. Profiles of the flow speed and pressure loss coefficient are as depicted in Fig. 30. Some new idea is necessary to remove the frost on the cooling tubes of this temperature range.

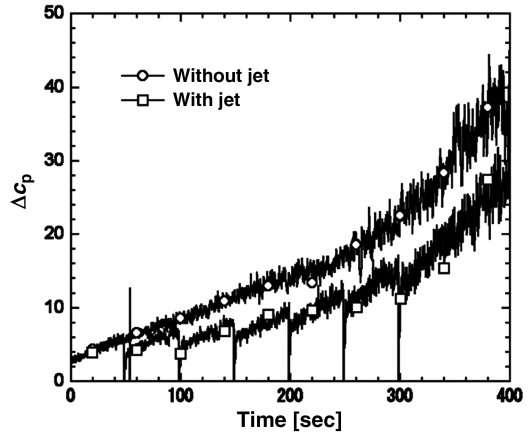

Fig. 29 Pressure loss coefficient with and without jet defrosting at the coolant temperature of 220 K.

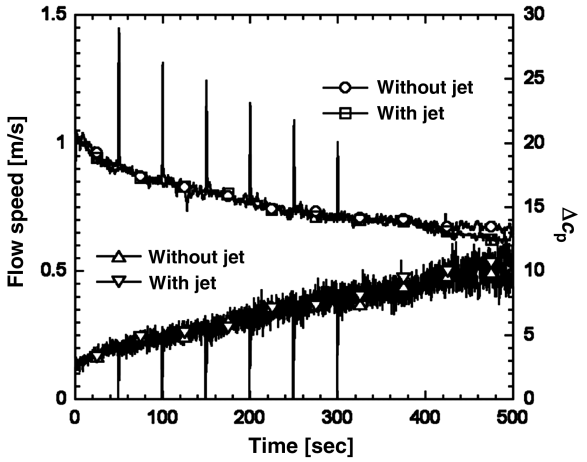

Fig. 30 Main airflow speed and the pressure loss coefficient profiles with and without jet defrosting at the coolant temperature of 250 K.

IV. Conclusions

The feasibility of a new defrosting method using jet impingement was experimentally investigated. The defrosting method is proposed for removal of the frost in a precooler installed in the gas turbine engine using cryogenic fuel. Effects of the main airflow speed and the coolant temperature on the effectiveness of the jet defrosting were studied through a fundamental experiment using one row cooling tubes.

The following conclusions were reached:

1) This defrosting method is effective when the main air flow speed is low (1.0 m/s) with low coolant temperature (83 K). The heat transfer rate and pressure loss are recovered by the jet impingement and become the same value as those at the test start.

(2) At the high flow speed (3.0 m/s) the defrosting method is less effective than at the low flow speed (1.0 m/s). However, in this condition the flowpath is not choked in the test duration of 500 s even if we do not use the defrosting method. This result is contrastive to that at 1.0 m/s, where the flowpath is choked in 250 s without the jet defrosting.

(3) At the high coolant temperature of 220 K the defrosting method is less effective than at 83 K. Moreover, at the coolant temperature of 250 K the defrosting method is not effective at all. However, at both coolant temperatures of 220 and 250 K, the flowpath is not choked in the test duration of 400 s even if we do not use the defrosting method. This is because the accumulation of the frost is much slower than that at 83 K.

In summary, this defrosting method is effective when the bad effects of frost are serious. Therefore, we conclude that this defrosting method is valuable.

Acknowledgments

The authors gratefully acknowledge Shujiro Sawai for his logistic support, which has enabled us to conduct this experiment. This research was also supported by a Grant-in-aid for scientific research (No. C19560793) provided by the Japan Society for the Promotion of Science.

References

[1] Sato, T., Taguchi, H., Kobayashi, H., Kojima, T., Okai, K., Fujita, K., Masaki, D., Hongoh, M., and Ohta, T., "Development Study of Precooled-Cycle Hypersonic Turbojet Engine for Flight Demonstration," *Acta Astronautica*, Vol. 61, Nos. 1–6, 2007, pp. 367–375. doi:10.1016/j.actaastro.2007.01.012

[2] Sato, T., Tanatsugu, N., Harada, K., Kobayashi, H., and Tomike, J., "Development Study on a Precooler for the Hypersonic Air-Breathing Engine," *Journal of the Japan Society for Aeronautical and Space Sciences*, Vol. 50, No. 580, 2002, pp. 196–203. doi:10.2322/jjsass.50.196

[3] Sato, T., Tanatsugu, N., Naruo, Y., Omi, J., Tomike, J., and Nishino, T., "Development Study on ATREX Engine," *Acta Astronautica*, Vol. 47, No. 11, 2000, pp. 799–808. doi:10.1016/S0094-5765(00)00129-6

[4] Hukusako, S., and Inaba, H., "Heat Transfer Phenomena in Low Temperature Environment and Its Application," Frost Formation and Its Fusion, Yokendo, Tokyo, 1996, pp. 240–278 (in Japanese).

[5] Japan Refrigerating Society Refrigerating and Air Conditioning Handbook Editing Committee, "Defrosting," *Refrigerating and Air Conditioning Handbook*, 4th ed., Japan Refridgerating Society, Tokyo, 1981, pp. 355–359 (in Japanese).

[6] Harada, K., Tanatsugu, N., and Sato, T., "Development Study of a Precooler for the Air-Turboramjet Expander-Cycle Engine," *Journal of Propulsion and Power*, Vol. 17, No. 6, 2001, pp. 1233–1238. doi:10.2514/2.5869

[7] Kimura, T., and Sato, T., "Improvement of the Precooler Performance Against the Icing Problem Using the Condensable Gas," *Journal of the Japan Society for Aeronautical and Space Sciences*, Vol. 51, No. 598, 2003, pp. 597–605. doi:10.2322/jjsass.51.597

[8] Sato, T., Tanatsugu, N., Kobayashi, H., Kimura, T., and Tomike, J., "Countermeasures Against the Icing Problem on the ATREX Precooler," *Acta Astronautica*, Vol. 54, No. 9, 2004, pp. 671–686. doi:10.1016/S0094-5765(03)00239-X

[9] Ohkubo, H., and Tajima, O., "Effect of Surface Temperature on Frosting Phenomena," *Transactions of the Japan Association of Refrigeration*, Vol. 12, No. 3, 1995, pp. 285–294 (in Japanese).

[10] Harada, K., "Study on Frost Formation in Heat Exchanger Using Cryogenic Coolant," Ph. D. Thesis, The University of Tokyo, Tokyo, 1999, pp. 78–139 (in Japanese).

[11] The American Society of Mechanical Engineering, Translated by the Japan Society of Mechanical Engineering, *Measurement Uncertainty*, ASME Performance Test Codes, Supplement on Instruments and Apparatus, The Japan Society of Mechanical Engineering, Tokyo, 1987, pp. 3–53 (in Japanese).

[12] Inaba, H., Horibe, A., and Kawakami, Y., "Defrost Behavior of Frost Layer Developed on Two Cooling Pipes by Sublimation Phenomenon," *Transactions of the Japan Society of Mechanical Engineers. B*, Vol. 66, No. 651, 2000, pp. 2964–2971 (in Japanese).